

Bragg transmittance of *s*-polarized waves through finite-thickness photonic crystals with a periodically corrugated interface

A. E. Serebryannikov,^{*} T. Magath,[†] and K. Schuenemann

Institut fuer Hochfrequenztechnik, Technische Universitaet Hamburg-Harburg, D-21071 Hamburg, Germany

(Received 26 December 2005; revised manuscript received 11 August 2006; published 14 December 2006)

Finite-thickness photonic crystals (PC's) with periodically corrugated interfaces are suggested to realize some unusual features in the behavior of transmitted Bragg beams (diffraction orders). The scattering of *s*-polarized plane waves by such structures is studied. It follows from the numerical results that rather thin corrugated PC's borrow their basic properties from both conventional PC's and gratings, leading to some new effects. In particular, a shift of the actual cutoff frequencies towards larger values than those of the Rayleigh cutoff frequencies can be obtained due to the ordinary opaque range in transmission, within which all propagative orders vanish. This effect can even be enhanced due to the nonordinary behavior arising at the edges of the ordinary opaque range, which manifests itself in that some but not all propagative orders in transmission are suppressed. Hence the opaque ranges for individual orders are wider than the corresponding ordinary range. Besides, frequency ranges exist which are not connected with the edge of the ordinary opaque range, where a similar nonordinary effect does appear. As a result, each propagative order in transmission generally has its own set of opaque ranges. Only a single order can be contributive while several others are formally propagative, too. The corrugations have to be located at the upper interface in order to realize these nonordinary effects. Moving the corrugation from the upper to the lower interface leads to a disappearance of the observed effects, so that their nature cannot be explained exclusively in terms of matching the wave vectors of the diffraction orders and the Floquet-Bloch waves. The conventional sequence of cutoffs for different diffraction orders with respect to each other can be changed for certain structures if the rods of a PC are made of Drude metal. Hence, transmission regimes can be realized which are beyond the classical theory of gratings. Several effects arising when varying the angle of incidence are demonstrated and briefly discussed. The detected effects can be used for controlling the number of actually contributive beams and for obtaining alternating ranges of single-beam and multibeam operation, which should lead to extending the potentials of optical and microwave technologies based on the use of single-beam and multibeam regimes.

DOI: [10.1103/PhysRevE.74.066607](https://doi.org/10.1103/PhysRevE.74.066607)

PACS number(s): 42.25.Fx, 42.70.Qs, 78.20.Ci

I. INTRODUCTION

Photonic crystals (PC's) have been the focus of interest during the last decade because of their unique abilities to control light propagation. A rich variety of interesting theoretical and experimental results has been reported for PC's of various types, which are concerned with the basic features of dispersion characteristics, transmission spectra, radiation of embedded sources, and so on—e.g., see [1–7]. One-, two-, and three-dimensional PC's made of dispersionless and dispersive materials have been considered. In the first two cases, great attention has been paid to the defect modes. Owing to strong frequency selectivity, they have been applied as working regimes in many devices like filters, splitters, tapers, fibers, waveguides, and cavities (see, for example, [8–12]). It has been shown that low- and zero-index [13–15], negative-index [16,17], and negative-index-like [5,18] behavior can be obtained in PC's without defects. These regimes are often associated with a number of such important applications like

directive radiation [6], wave front controlling [15], and lensing [19,20]. Besides, collimation and superprism effects have been demonstrated in PC's [2].

In most of the theoretical considerations and applications of two-dimensional finite-thickness PC's, structures with linear interfaces have been studied—i.e., when all layers are in parallel and identical. The same holds for a large portion of PC's with line defects, for which equivalent linear interfaces could be introduced. Less attention has been paid to PC's with curvilinear (inner and outer) interfaces. In particular, the idea of an add and drop PC filter with ring-shaped defect has been suggested and expected diffraction effects for a curvilinear nonperiodic surface of a two-dimensional PC have been mentioned in [8]. PC's with curvilinear interfaces have been used as planoconcave lenses [14,21]. They can also be used in the inverse regime—i.e., to obtain flat wave fronts from a point source. Shifting some rods at an outer interface of the PC has been proposed in [22] as a tool for improving beam-shaping abilities at the open end of a PC waveguide. Curvilinear concave and convex interfaces have been used in the dual lattice PC beam splitter [23] and in the curved-bend waveguide [24]. Besides, quasiperiodic circular PC's have been reported in [2], for which a circular interface can be introduced. In principle, some types of PC fibers can also be assigned to PC's with curvilinear equivalent interfaces (e.g., [2,9]). In this context, one should also mention PC prisms [14,16] and tapers [25], which show piecewise-linear interfaces.

^{*}On leave from the Institute of Radio Astronomy, National Academy of Sciences of Ukraine, Kharkiv, Ukraine. Electronic address: serebryannikov@tu-harburg.de

[†]Present address: PEDEU-TC (European Technology Center), Panasonic Electronic Devices Europe GmbH, D-21337 Lueneburg, Germany.

On the other hand, various structures with curvilinear interfaces made of homogeneous metamaterials are considered to be promising for realizing some physical effects [26–30]. In particular, scattering by structures with periodically corrugated interfaces (gratings) has been studied in [28–30]. The properties of the materials considered in these studies are expected to be obtainable using PC's, too, at least within a narrow range of variation of the frequency and/or the angle of incidence.

Although any two-dimensional finite-thickness PC with linear interfaces is nothing else than a grating of special configuration, only some aspects of the regimes associated with the simultaneous presence of more than one propagative diffraction order have been discussed—e.g., see [1, 16, 31–33]. It is worth noting that the lowest gap of the dispersion characteristic usually appears at lower frequencies than those starting from which at least one higher order becomes propagative. At the same time, although Floquet-Bloch (FB) waves inside a PC remain the same whatever the interface, even a variation of the orientation of a part of the piecewise-linear interface can lead to a strong variation in the behavior of the beams inside the PC [34]. It is natural to expect that a similar strong sensitivity will appear when introducing more complicated interfaces and that it would be pronounced in the transmission characteristics.

Our idea is to change the geometrical configuration of a two-dimensional finite-thickness PC in such a manner that the frequency range, where higher orders (multibeam regime) might appear, is shifted towards lower frequencies, up to those values which correspond to the lowest opaque range in transmission. In this paper, we present a collection of the effects arising in transmission owing to the one-dimensional gratinglike periodic modulation, which is obtained by removing some rods at one of the interfaces of a regular PC. We expect that the suggested structure will show intermediate, in some sense, behavior between that of a conventional dielectric grating and that of a PC. Two-dimensional PC's are considered, which are composed of dielectric or metallic rods arranged in a square lattice. Most of the results presented have been obtained for sinusoidal corrugation. Both cases of an air and of a dielectric host medium will be studied. The emphasis in the numerical study will be put on searching for transmission regimes, which are unusual for conventional PC's and gratings.

Along with the band gaps of the dispersion characteristic and with uncoupled modes, which are the main causes of the appearance of opaque ranges in transmission [1], the presence of cutoff frequencies and angles for diffraction orders [35] should be a basic feature determining the dominant properties of the structures considered. These cutoffs occur for any periodic structure, including noncorrugated PC's. However, we shift them towards smaller frequencies owing to the corrugation. We restrict our consideration to rather thin PC's, where the thickness effect and the evanescent waves might contribute to the observed features. Because of this, we pay the main attention to the study of transmission, while that of dispersion characteristics is omitted. Instead, we consider transmission through the corresponding noncorrugated PC with the same number of layers as a benchmark.

Contrary to Ref. [33] where various combinations of the number of beams above the PC-air interface and inside the

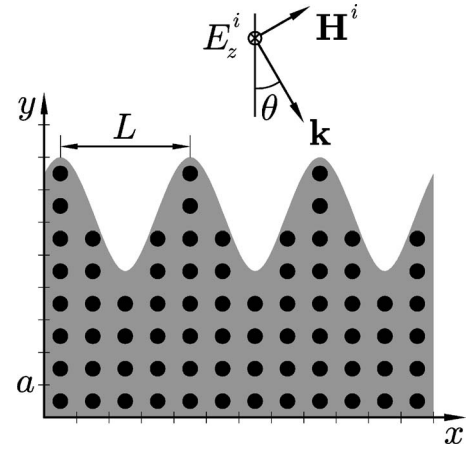


FIG. 1. PC with periodically corrugated upper interface.

PC have been demonstrated, we will show that a similar property can be realized in transmission through a finite-thickness corrugated PC: The number of actually contributive beams in transmission and reflection can be different. The presented numerical results have been obtained using the recently developed fast coupled-integral-equations technique [36].

II. THEORETICAL BACKGROUND

Assume that an *s*-polarized plane wave is incident on the periodic structure from the side of positive *y*—i.e.,

$$E^i(x, y) = E_0^i \exp(i\alpha_0 x - i\eta_0 y), \quad (1)$$

where $\alpha_0 = k \sin \theta$, $\eta_0 = k \cos \theta$, k is a free-space wave number, θ is the angle of incidence, and E_0^i means amplitude. The structure represents a finite-thickness, two-dimensional, square-lattice PC with a corrugated interface (see Fig. 1).

The field in the half-spaces above ($y > Na$, a is a lattice constant, N is the number of layers) and below ($y < 0$) the PC is presented as the superposition of an infinite number of diffraction (grating) orders as follows:

$$E(x, y) = E^i(x, y) + \sum_{n=-\infty}^{\infty} \rho_n \exp(i\alpha_n x + i\eta_n y), \quad (2)$$

$$E(x, y) = \sum_{n=-\infty}^{\infty} \tau_n \exp(i\alpha_n x - i\eta_n y), \quad (3)$$

where $\eta_n = \sqrt{k^2 - \alpha_n^2}$, $\text{Im}\{\eta_n\} \geq 0$, $\alpha_n = \alpha_0 + 2\pi n/L$, L is the modulation period, and ρ_n and τ_n are Fourier amplitudes of n th order in reflection R_n and transmission T_n , respectively. If the incident wave is a wide beam with its waist $w \gg L$, the scattered field represents a finite number of wide (Bragg) beams, each of which is associated with a separate order R_n or T_n .

The n th-order beams are propagative if $\text{Re}\{\eta_n\} > 0$ and $\text{Im}\{\eta_n\} = 0$ —i.e., if

$$k > |\alpha_0 + 2\pi n/L|. \quad (4)$$

We denote the cutoff value of k , which splits the propagating- and evanescent-wave regimes above and below the periodic structure and hence corresponds to the Rayleigh frequency for R_n and T_n , by

$$k_c^n(L, \theta) = \frac{2\pi|n|}{L(1 \pm |\sin \theta|)}, \quad (5)$$

where the signs + and – correspond to the cases with $\text{sgn } n \neq \text{sgn } \theta$ and $\text{sgn } n = \text{sgn } \theta$, respectively (see [35]). The angles of diffraction of the n th-order reflected and transmitted beams are given by

$$\sin \phi_n(L) = -(\sin \theta + 2\pi n/kL) \quad (6)$$

and

$$\hat{\phi}_n(L) = \pi - \phi_n(L), \quad (7)$$

respectively. They correspond to Eq. (5) and determine the propagation directions of individual beams at fixed kL . It is assumed that ϕ_n is measured from the y axis in a counter clockwise direction.

For the noncorrugated PC, we have

$$k_c^n(a, \theta) = \frac{2\pi|n|}{a(1 \pm |\sin \theta|)}, \quad (8)$$

instead of Eq. (5) and hence $k_c^n(L, \theta) < k_c^n(a, \theta)$, while L is replaced by a in Eqs. (6) and (7). It is known from numerous theoretical considerations that the condition

$$\chi_u \approx \hat{\chi}_u < k_c^{-1}(a, \theta),$$

where $\hat{\chi}_u$ and χ_u are the upper boundaries of the lowest band gap of the dispersion characteristic and of the corresponding opaque range in transmission, respectively, is usually satisfied in a wide range of positive θ . In many cases, the factor $F(\theta) = \hat{\chi}_u/k_c^{-1}(a, \theta)$, which depends on geometrical and material characteristics of the PC, is substantially smaller than 1. For example, $F(0) < 0.32$ in the cases presented in [2], p. 48, and in [37,38], and $F(0) < 0.45$ in [39]. On the other hand, the ratio $\hat{\chi}_l/k_c^{-1}(a, 0)$, where $\hat{\chi}_l$ is the lower boundary of the lowest band gap, can take values starting at least from 0.18. Note that $F(0) = 0.32$ and 0.45 correspond to $F(\pi/4) = 0.55$ and 0.77 and to $F(\pi/3) \approx 0.6$ and 0.84 , respectively. These examples correspond to typical situations when the first or several first opaque ranges appear while all higher orders ($|n| > 0$) are evanescent.

To realize the multibeam regime within a kL range involving the first (lowest) opaque range, or at least one of its edges, we take a PC with linear interfaces at $y=0$ and $y=Na$ and then introduce a periodic corrugation by cutting a part of it from the side of one of the interfaces. In Fig. 1, such geometry with corrugated upper interface is shown. It is assumed that

$$L = ma, \quad (9)$$

where $m=2, 3, 4, \dots$. Owing to the corrugation, the range of k variation, where higher-order beams are allowed to propa-

gate, is shifted towards smaller k values, so that the case with

$$k_c^{-1}(L, \theta) < \chi_l, \quad (10)$$

where χ_l is the lower boundary of the first opaque range, or that with

$$\chi_l < k_c^{-1}(L, \theta) < \chi_u \quad (11)$$

is expected to be obtained. The contribution of higher orders to the transmission and/or reflection should be controllable by a proper choice of the corrugation shape.

We use the following coordinate dependence for the permittivity:

$$\varepsilon(x, y) = G(x, y)P(x, y)Q(x, y). \quad (12)$$

Here G sets geometrical and material parameters of the large-period host-dielectric grating (shown in gray in Fig. 1), P is the function introducing the rods into the host, and Q is the correcting factor which is responsible for the rods, which should be crossed by an interface, not being inserted. Assume that the following periodicity conditions are satisfied: $G(x+a, y) = G(x, y)$, $P(x+L, y) = P(x, y)$, and $Q(x+L, y) = Q(x, y)$. Then,

$$\varepsilon(x+L, y) = \varepsilon(x, y).$$

The function $G(x, y) = \varepsilon_h$ at $f_0(x) < y < f_1(x)$ and $G(x, y) = \varepsilon_0$ at $y > f_1(x)$ and $y < f_0(x)$, where ε_h and ε_0 mean relative permittivities of the host medium and free space, respectively, and f_0 and f_1 set the lower and upper interfaces. Taking $\varepsilon(x, y) = G(x, y)$, we obtain a similar structure as in Fig. 1, but without the rods inserted, so that the whole region between $y=f_0(x)$ and $y=f_1(x)$ would be shown in gray.

To set the values of $P(x, y)$, we take $P(x, y) = \varepsilon_r/\varepsilon_h$ if $\tilde{x}^2 + \tilde{y}^2 \leq d^2/4$ and $f_0(x) < y < f_1(x)$ and $P(x, y) = 1$ otherwise. Here ε_r and d mean the relative permittivity and diameter of the rods, respectively, $\tilde{x} = x - (j-1/2)a$ with $j=1, 2, \dots, m$ and $\tilde{y} = y - (l-1/2)a$ with $l=1, 2, \dots, N$. Multiplying $G(x, y)$ by $P(x, y)$, we insert the rods into the host. However, some of them can be crossed by the interface. To not insert such rods, we use an additional correcting factor $Q(x, y) = Q_{lj} = \varepsilon_h/\varepsilon_r$ within the (l, j) th rod, if it is crossed by f_1 or f_0 , and $Q(x, y) = 1$ otherwise.

Note that our structure is double-periodic along the x axis and single-periodic along the y axis. Hence it belongs to another type of periodic structures than the double-periodic structures considered in [2], Chap. 8. The transmission properties are expected to be determined by a common effect of all periodicities, while the contribution of each of the orders should depend on the corrugation shape. Considering two limiting cases—i.e., (i) with d/a tending to 0 and (ii) with $f_0(x)=0$, $f_1(x)=Na$ and $\varepsilon_r \neq \varepsilon_h$ —we intuitively arrive at the following condition for the actual cutoff for the n th order κ_c^n :

$$k_c^n(a, \theta) \geq \kappa_c^n(\theta) \geq k_c^n(L, \theta). \quad (13)$$

The modification of the PC used can also be interpreted as introducing the periodic defects at the interface(s). Then the structures considered are distinguished from most of the known PC's with defects, where all or at least most part of them are isolated from the interfaces by regular layers. In the

numerical examples, we assume that the host medium at $f_0(x) < y < f_1(x)$ is a lossless dielectric with $\varepsilon_h \geq 1$, while the rods are fabricated from either a lossless dielectric with $\varepsilon_r \neq \varepsilon_h$ or a metal. In the latter case,

$$\varepsilon_r = 1 - \omega_p^2 / [\omega(\omega + i\gamma)], \quad (14)$$

which corresponds to Drude's model. Here ω_p and γ mean plasma and collision frequencies, respectively. The results presented below for the metallic rods can also be used in the case that each of the rods models a circular cluster of rods of smaller diameter and each cluster effectively behaves like a portion of a Drude medium with $\omega_{p,eff} < \omega_p$ (see [40]).

To characterize transmission and reflection in a multibeam regime, we consider the energy distribution between the propagative orders R_n and T_n . According to [35], the diffraction efficiencies (DE's) in reflection (r_n) and transmission (t_n) are equal to a part of the total energy taken by the orders R_n and T_n , respectively—i.e.,

$$r_n = \text{Re}\{\eta_n \rho_n \rho_n^* / \mathcal{W}\}, \quad (15)$$

$$t_n = \text{Re}\{\eta_n \tau_n \tau_n^* / \mathcal{W}\}, \quad (16)$$

where \mathcal{W} is the energy of the incident wave and the asterisk means complex conjugation. In the lossless case,

$$\mathcal{R} + \mathcal{T} = \mathcal{W},$$

where the reflectance $\mathcal{R} = \sum_{n=-\infty}^{\infty} r_n$ and the transmittance $\mathcal{T} = \sum_{n=-\infty}^{\infty} t_n$. We refer to a partial transmittance and partial reflectance, which correspond to t_n and r_n , as to the n th-order Bragg transmittance and reflectance, respectively. For definiteness, we state that the order T_n or R_n is suppressed if $u_n / \mathcal{W} \leq 2.5 \times 10^{-3}$ where u_n means either t_n or r_n . The value of $\kappa_c^n(\theta)$ is a minimal k , at which the equality in this condition is achieved.

As is known, each wave propagating inside the PC has a form of a FB wave—e.g., see [1,33]. At the PC-air (noncorrugated) interface, the number of reflected beams associated with the grating orders and the total number of the transmitted ($n=0$) and higher-order refracted ($|n| > 0$) beams inside the PC which are associated with FB waves can show a variety of combinations [33]. Despite the fact that the conditions of the appearance of the required number of beams inside the PC and below the conventional relief grating are different, the possible nonequality of the above-mentioned numbers looks like a general property [41]. Contrary to [33], we are mainly interested in transmission through a finite-thickness PC, so that the consideration in terms of DE's is quite reasonable. It is furthermore so because the minimal thickness of the structures considered is $4a$, so that the effects in transmission, which are related to the finite thickness, cannot be neglected. At the same time, we analyze the near-field patterns to better understand the transmission mechanism.

III. NUMERICAL RESULTS AND DISCUSSION

Now we demonstrate the basic effects arising in transmission through the PC's due to introducing corrugation at either

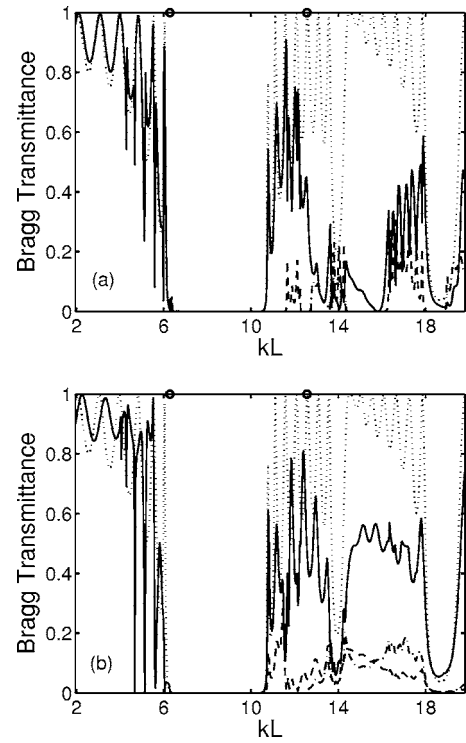


FIG. 2. Transmission with different Bragg beams through a PC with each fourth ($L=4a$) rod removed (a) from the most upper and (b) from the lowest line of the rods at $\varepsilon_r=11.4$, $\varepsilon_h=1.0$, $d/a=0.4$, $N=8$, and $\theta=0$. Thick solid, dashed, and dash-dotted lines correspond to t_0 , $t_{\pm 1}$, and $t_{\pm 2}$, respectively; the thin dotted line shows \mathcal{T} for a PC with noncorrugated interfaces. Open circles show the values of $k_c^n(L, \theta)$ at $n = \pm 1$ and ± 2 .

the upper or lower interface for both cases of dielectric and metallic rods. For all examples, $\omega a / 2\pi c < 0.8$. The DE values of some propagating orders—i.e., $T_{\pm 3}$ at $\theta=0$ and $T_{-3,-4}$ at $\theta > 0$ —are not shown, since they do not affect the features demonstrated. In all cases considered, $m=4$.

A. Purely dielectric structures

First, the simplest corrugation is considered, which appears due to removing each m th rod from either the most upper, the N th, or the lowest, 1st, line of the rods. The dependence of t_n on kL is shown for this case in Fig. 2. For comparison, $\mathcal{T}=t_0$ is shown for the noncorrugated PC with $N=8$, for which the lowest higher-order beams ($n = \pm 1$) may appear starting from $kL=8\pi$. One can see that the ranges of opaque \mathcal{T} for the corrugated and noncorrugated PC's almost coincide regardless of which side is corrugated. While all propagative beams ($n=0, \pm 1$) simultaneously appear at the right edge of the first opaque range of \mathcal{T} ($kL=10.6$), if the lower interface is corrugated, only the 0th order is not suppressed, if the upper interface is corrugated. Hence nonordinary behavior can arise at the edge, which manifests itself in the fact that certain formally propagative beams are suppressed, so that the opaque ranges of individual beams can be extended beyond the common opaque range. In particular, in Fig. 2(a), t_0 exclusively contributes to \mathcal{T} at $10.6 < kL$

< 11.6 . In Fig. 2(b), this effect is absent. Furthermore, kL ranges were found, where only T_0 is not suppressed and which are not an extension of the opaque range of \mathcal{T} . In Fig. 2(a), such ranges are observed at $12.3 < kL < 12.8$ and at $14.4 < kL < 16.3$. Similar but wider ranges occur for $T_{\pm 1}$ and $T_{\pm 2}$. Further we refer to the ranges where several but not all of the propagative beams T_n are suppressed as to the *nonordinary opaque ranges*, in contrast with the ordinary opaque ranges, where all propagative beams are suppressed simultaneously.

On the other hand, we call an extension of the opaque range for a certain T_n in comparison with the opaque range of \mathcal{T} the *nonordinary behavior at the edge of the ordinary opaque range*. From the presented results it follows that *each order (or pair of the orders if $\theta=0$) has its own opaque range*, which can coincide in part with the ordinary opaque range of \mathcal{T} . It is seen that the presence of corrugations of the upper interface is necessary for the appearance of a nonordinary range and nonordinary behavior at the edge. Since the propagating FB waves inside the PC are the same whatever the interfaces are, the observed suppression is undoubtedly connected with the location of the corrugation surface. Note that the ordinary opaque ranges in Figs. 2(a) and 2(b) are related to the first band gap of the dispersion characteristic. This remains true for all other examples presented in this section.

The observed type of suppression has nothing to do with the conventional Rayleigh cutoffs, a basic effect known from the theory of gratings [35]. Indeed, those orders T_n are suppressed, which are propagative according to (4). The second important effect is a *shift of the actual cutoffs* of individual orders towards larger kL as compared to the cutoffs given by (4). This effect appears due to the combination of Rayleigh cutoffs and opaque ranges. Obviously, it can be obtained even for the ordinary opaque range. For example, although weak peaks of $T_{\pm 1}$ are observed in Fig. 2(a) in the vicinity of $\chi_{lL} \approx 6.42$, the actual cutoff for the beams with $n = \pm 1$ should be assigned at least to the right edge—i.e., $\kappa_c^{\pm 1}(L, 0) = \chi_{lu} \approx 10.6$. (Here and further we use the notation κ_c^n for the orders T_n only.) However, the actual cutoff is even more shifted towards larger kL due to the nonordinary behavior arising at the right edge, so that $\kappa_c^{\pm 1}(L, 0) > \chi_{lu}$. The detected effects give a new possibility to control the number of diffraction orders which actually contribute to \mathcal{T} .

Figure 3 demonstrates the effect on the near-field pattern exerted by moving the corrugations from the upper to the lower interface. One can see that the ability of the noncorrugated PC to transfer flat wave fronts at these parameters is not affected by removing rods from the upper interface. In this case, the transmitted field is affected by the corrugations only in that the value of $\mathcal{T} \approx t_0$ can be varied. On the contrary, if some rods are removed from the lower interface, the field distribution over x at $y < 0$ takes more features related to the large period and hence higher orders are forced to be pronounced in \mathcal{T} . It is worth noting that for the noncorrugated PC with the same parameters as in Figs. 2 and 3, no nonordinary effect has been observed at those (larger) kL , for which the orders with $n = \pm 1$ and ± 2 are propagative, while the boundaries of the opaque ranges corresponding to the individual orders have (almost) coincided in the same man-

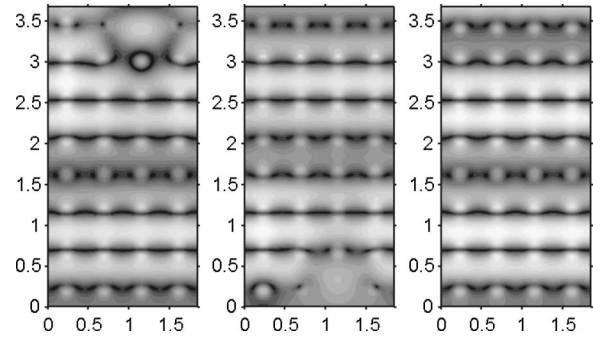


FIG. 3. Electric field distribution within the region $0 \leq x \leq L$, $0 \leq y \leq Na$ in the vicinity of the right edge of the first opaque range of \mathcal{T} in Fig. 2 at $kL=11.2$. Left and middle plots correspond to the corrugated PC's from Figs. 2(a) and 2(b), respectively. Right plot: noncorrugated PC at the same kL . Brighter regions correspond to larger field values, $\max|E|/|E_0^i| \approx 3$. Most dark regions in this and other figures showing field patterns correspond to (almost) zero-field values.

ner as for the corrugated PC in Fig. 2(b). Such a coincidence is typical for the noncorrugated PC's and remains present in a wide range of the variation of kL , θ , and ϵ_r .

The strength of the nonordinary effects observed in Fig. 2 can be controlled by varying the corrugation shape. Figure 4 shows the basic features in the behavior of t_n vs kL in the case of a sinusoidally modulated interface when

$$f_1 = Na[A + B \cos(2\pi x/L + \varphi_1)], \quad (17)$$

$$f_0 = Na[C + D \cos(2\pi x/L + \varphi_0)], \quad (18)$$

where A , B , C , D , φ_0 , and φ_1 are chosen in such a way that the corrugation is either similar to that in Fig. 1 [for Fig. 4(a)] or inverse to it; i.e., the structure has been rotated by 180° [for Fig. 4(b)]. In contrast with Fig. 2(a), t_0 dominates in \mathcal{W} in Fig. 4(a) within the nonordinary opaque range, $14.3 < kL < 16.1$. It is interesting that the location of the corrugations affects the kL dependence of t_0 within this range just weakly, while for higher-order beams it is very important: Corrugations enhance either T_n or R_n , $|n| > 0$, if they are located at either the lower or upper interface, respectively. This leads, in particular, to the \mathcal{T} value being larger in Fig. 4(b) than in Fig. 4(a), at least within the considered nonordinary range.

Figure 5 shows r_n vs kL at the same parameters as in Fig. 4. In case (a), there is no analog of the nonordinary opaque range for the reflection. All propagative orders—i.e., R_0 and $R_{\pm 1}$ —contribute to \mathcal{R} within the ordinary opaque range of \mathcal{T} . The exceptions take place in the vicinity of $kL=7.2$ and of $kL=8.7$ where $r_0=1$. In case (b), R_n at $|n| > 0$ are not suppressed only within narrow ranges of kL variation, so that wide ranges between them can be considered as the nonordinary opaque ranges.

It is worth noting the appearance of subranges with non-zero \mathcal{T} in the case of the corrugated PC, at kL values corresponding to the opaque range of \mathcal{T} arising in case of the noncorrugated PC at the same θ . For example, they are observed at both edges of the opaque range of \mathcal{T} in Fig. 4(a).

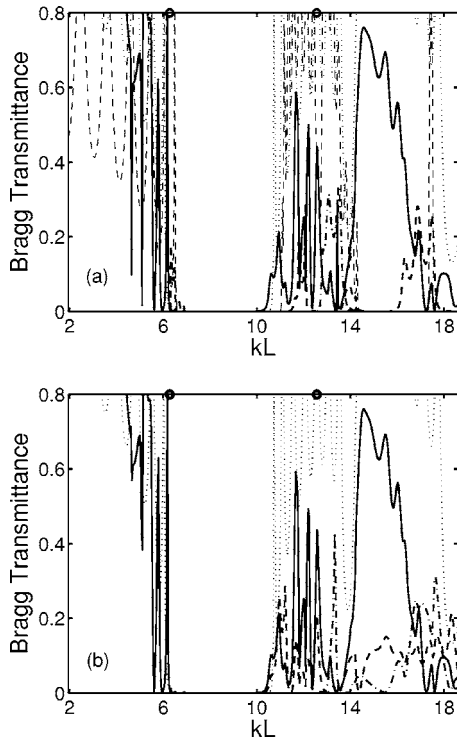


FIG. 4. Transmission with different Bragg beams in the case when one of the interfaces is sinusoidally corrugated: $\varepsilon_r=11.4$, $\varepsilon_h=1.0$, $d/a=0.4$, $N=8$, $\theta=0$, $L=4a$, and $\varphi_0=\varphi_1=-\pi/4$. (a) Upper corrugated interface: $A=0.79$, $B=0.21$, and $C=D=0$. (b) Lower corrugated interface: $A=1$, $B=0$, and $C=D=0.21$. Thick solid, dashed, and dash-dotted lines correspond to t_0 , $t_{\pm 1}$, and $t_{\pm 2}$, respectively; thin dotted and dashed lines show t_0 for the noncorrugated PC at $\theta=0$ and $\theta=\pi/3$, respectively; open circles show the values of $k_c^n(L,0)$ at $n=\pm 1$ and ± 2 .

We expect that there are at least two possible reasons for the appearance of this effect: (i) the presence of incomplete gaps in the dispersion characteristic, where propagation inside an infinite PC is forbidden for a certain range of directions only, which can correspond to a limited θ range of nonzero \mathcal{T} , while value(s) of $-\phi_n$, $|n|>0$ belong to this range but $-\phi_0$ does not, and (ii) tunneling of a (non) enhanced wave through a rather thin PC. A detailed study of physical scenarios of transmission through the corrugated PC's within the opaque ranges of the corresponding noncorrugated PC's is a subject of further studies. Here we just give some illustrations.

Figure 6 shows the field patterns at the left edge of the ordinary (lowest) opaque range for both the corrugated and noncorrugated PC's from Fig. 4(a). In the left plot, the field corresponds to the peak of $t_{\pm 1} \approx 0.18$ observed at the edge, in the case with corrugations. It arises at that kL value which belongs to the opaque range of \mathcal{T} for the corresponding noncorrugated PC with $N=8$ at $\theta=0$ (see the middle plot). However, rather substantial transmission still occurs at larger θ —e.g., at $\theta=\pi/3$ where $\mathcal{T} \approx 0.07$ (see the right plot). On the other hand, for the corrugated PC in Fig. 4(a), at the last peak of t_0 before the opaque range, $kL \approx 6.17$, the field shows similar features to those in the left plot in Fig. 6. At the last peak of t_0 for the noncorrugated PC at $\theta=\pi/3$, $kL \approx 6.49$, the

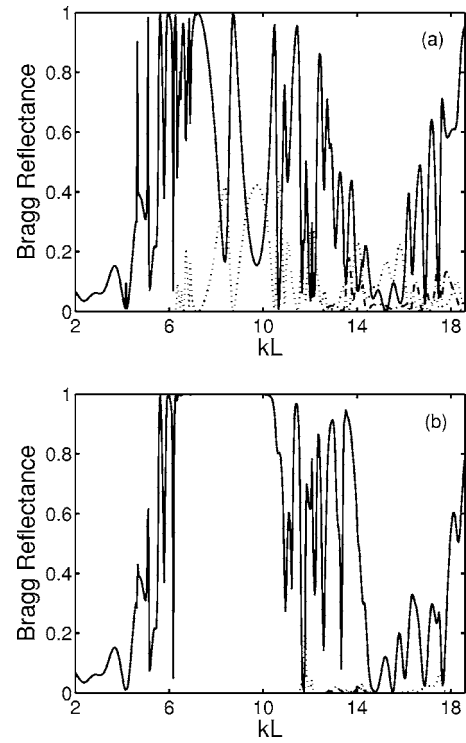


FIG. 5. Reflection with different Bragg beams at the same parameters as in Figs. 4(a) and 4(b), respectively. Thick solid, dotted, and dash-dotted lines show r_0 , $r_{\pm 1}$, and $r_{\pm 2}$, respectively.

field is similar to that in the right plot in Fig. 6. Hence, in contrast with Fig. 3, the field in cases with corrugations is not a locally perturbed version of that in the case without corrugations. Although the transmission mechanism like that shown in the left plot in Fig. 6 is not yet completely understood, it is clear from the comparison of the corrugated and noncorrugated PC's that it is connected with the presence of corrugations. Probably, this mechanism is realized due to peculiar eigenmodes of the entire finite-thickness structure.

The extent to which this effect is pronounced depends on the corrugation shape. For example, a similar peak of $t_{\pm 1}$ is observed in the case with $N=16$, $\min N_j=8$, and the same other parameters as in Fig. 4(a), and tends to disappear once

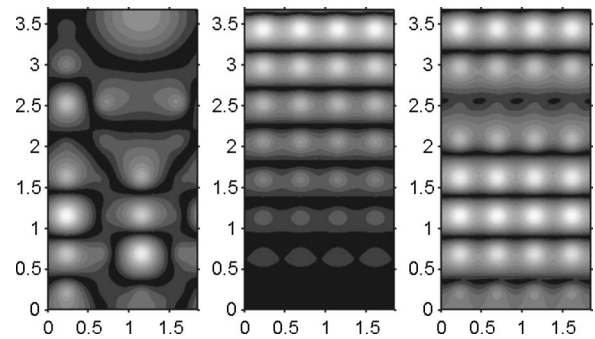


FIG. 6. Electric field within region $0 \leq x \leq L$, $0 \leq y \leq Na$ at $kL = 6.34$ and parameters for the corrugated PC from Fig. 4(a) (left) and for the noncorrugated PC from Fig. 4(a) at $\theta=0$ (middle) and $\theta=\pi/3$ (right); brighter regions correspond to larger field values, $\max|E|/|E_0| \approx 8.8$ (left), 1.3 (middle), and 0.9 (right).

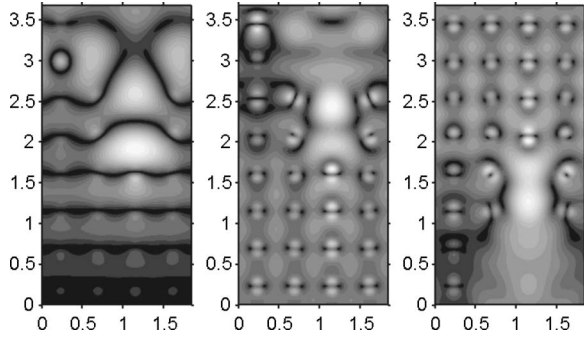


FIG. 7. Electric field within the region $0 \leq x \leq L$, $0 \leq y \leq Na$ at $kL=10.55$ (left) and parameters for the corrugated PC from Fig. 4(a); at $kL=14.58$ and parameters for the corrugated PC's from Figs. 4(a) (middle) and 4(b) (right), respectively; $\max|E|/|E_0^i| \approx 6.2$ (left), 3.2 (middle), and 3.4 (right).

$\min N_j$ is increased (i.e., A is increased while $A+B=1$). In Fig. 2(a), two very weak peaks appear at the right edge at $kL=6.3$ and 6.37 .

The left plot in Fig. 7 corresponds to the situation when the propagative orders $T_{\pm 1}$ are suppressed and $kL \approx \tilde{\chi}_u^{(nc)} L < \hat{\chi}_u^{(nc)} L$, where $\tilde{\chi}_u^{(nc)}$ and $\hat{\chi}_u^{(nc)}$ are the upper boundaries of the lowest opaque range for noncorrugated PC's with $N=4$ and $N=8$, respectively. However, T for the corrugated PC is substantially larger than for the noncorrugated PC with $N=4$. This occurs because the tunneled field is first enhanced due to the effect of the groove. This effect looks similar to the effect of the resonant tunneling of light via strongly localized surface plasmons, which has been observed for thin metal films with corrugated interfaces [42]. Such a regime can be considered as a surface defect mode. At $\hat{\chi}_u^{(nc)} L < kL < 11.5$, where $T_{\pm 1}$ are also suppressed, the transmission mechanism is the same as in Fig. 3. It is realized in the cases shown in the middle and right plots in Fig. 7 for either the upper or lower corrugated interface. These two cases correspond to a kL value taken from the nonordinary opaque range in Fig. 4(a). Similarly to Fig. 3, the presence or absence of higher orders within this range in Fig. 4 cannot be explained in terms of matching the wave vectors of FB waves and diffraction orders: Modification of the field arising due to corrugations seems to be the dominant factor for the presence of contributive higher-order beams in either the reflected or transmitted field.

As follows from the obtained results, the dependence of $\chi_l L$ and $\chi_u L$ on θ occurs for the noncorrugated PC, according to which transmission can be possible within a certain range of the “allowed” angles. This dependence can serve as a signature of the nonordinary behavior at the edge for the corrugated PC whatever the transmission mechanism is. The following approximate *rule* can be formulated: Those diffraction orders are expected to dominate in the transmission through the corrugated PC, at a given kL , for which $-\phi_n(L)$ is closer to such θ values at which transmission through the noncorrugated PC remains significant, while for another θ it tends to vanish, provided that only T_0 and R_0 are propagative for the noncorrugated PC. For example, $\phi_{\pm 1}(L) = \mp 82.3^\circ$ at $kL=6.34$ where $T_{\pm 1}$ are only present and $\phi_{\pm 1}(L) = \mp 35^\circ$ at $\tilde{\chi}_u^{(nc)}(0)L < kL = 10.95 < \hat{\chi}_u^{(nc)}(\pi/3)L$ where $T_{\pm 1}$ are suppressed [see Fig. 4(a)].

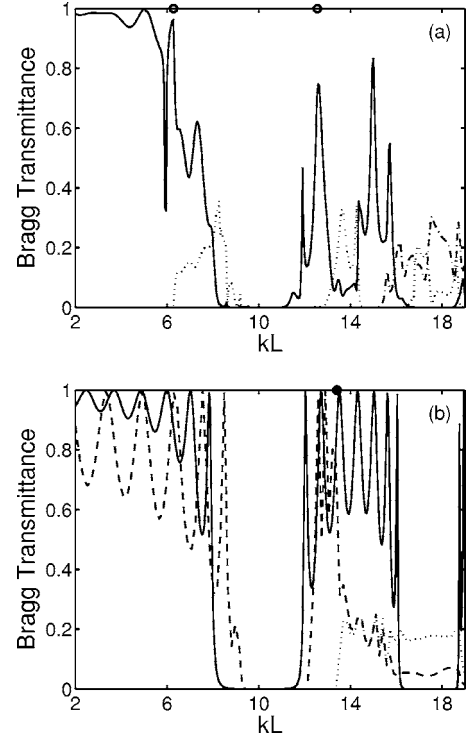


FIG. 8. Transmission with different Bragg beams through a PC with $\epsilon_r=5.8$ and $\epsilon_h=1.0$. Case (a): geometrical parameters and θ are the same as for the corrugated PC in Fig. 4(a); solid, dotted, and dash-dotted lines correspond to t_0 , $t_{\pm 1}$, and $t_{\pm 2}$, respectively; open circles show the values of $k_c^n(L, 0)$ at $n=\pm 1$ and ± 2 . Case (b): geometrical parameters are the same as for the noncorrugated PC in Fig. 4(a); solid, dashed, and dotted lines show $T=t_0$ at $\theta=0$, t_0 , and t_{-1} at $\theta=\pi/3$, respectively; the solid circle shows $k_c^{-1}(a, \pi/3)$.

The manifestation of the above-discussed effects can also be controlled by an appropriate choice of the permittivity values. Figure 8(a) demonstrates the effect of decreasing ϵ_r , while other parameters are taken from Fig. 4(a). Figure 8(b) shows t_n for the noncorrugated PC with $N=8$ at two values of θ . Comparing the cases (a) and (b), one can see that the prevalence of one of the orders at the edges again correlates with locations of the edges of the opaque ranges of the noncorrugated PC at different θ , as has just been discussed. Furthermore, such correlation occurs at $16.9 < kL < 18.3$, where the nonordinary opaque range of another kind is seen in Fig 8(a), within which the propagative order T_0 is only suppressed. Hence only deflected beams are actually contributive to T in this case.

Replacing the air host medium by a dielectric one, even with low ϵ_h , results in a substantial change of the t_n values. In Fig. 9, $\epsilon_h=2.1$ is used, which leads to a shift of the ordinary opaque range towards smaller kL . Contrary to Fig. 4(a), there are several opaque ranges for the noncorrugated PC. However, only the first of them is associated with the ordinary opaque range of the corrugated PC. The most part of the second one corresponds to the nonordinary range with suppressed T_0 , which extends from $kL=11.6$ to 13.2 . Furthermore, at $11.6 < kL < 4\pi$, the transmission is exclusively realized due to the deflected beams $T_{\pm 1}$. Here $\phi_{\pm 1}(L) = \mp 31.6^\circ$ at $kL=12$ —i.e., near the left edge of the region

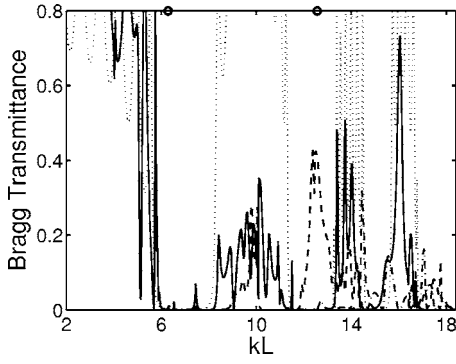


FIG. 9. Same as Fig. 4(a) but for $\varepsilon_h=2.1$. The geometry of the corrugated PC is almost the same as in Fig. 1.

where only $t_{\pm 1}$ show nonzero values. This situation is similar to that observed in Fig. 8(a), but here we have only two beams. Besides, isolated peaks of t_0 occur within the ordinary opaque ranges, for example, at $kL=7.44$ and $kL=11.5$, which are typical for the conventional defect modes, as well as the corresponding field patterns.

Figure 10 shows three typical examples of the near-field pattern for the parameters from Figs. 8(a) and 9. The left plot corresponds to the nonordinary opaque range in Fig. 8(a), where T_0 is suppressed. The middle plot shows the field for the noncorrugated PC at the same kL and $\theta=21.7^\circ$, which corresponds to $\phi_{\pm 1} \approx 0$ in the left plot. From the comparison, one can see that the role played by corrugation is here to provide such a field topology that, at least within a part of the considered region, it is rather similar to that of the noncorrugated PC obtained but at a rather large θ , at which nonzero T is possible in contrast with the vicinity of $\theta=0$. The right plot corresponds to the peak of t_0 arising within the lowest ordinary opaque range in Fig. 9. This regime belongs to the defect modes.

The above-described effects have also been observed at nonzero θ (see Fig. 11). However, contrary to Figs. 4(a) and 9, higher-order beams dominate at the right edge and the zeroth-order beam does so at the left edge of the lowest ordinary opaque range. This is in agreement with the above-

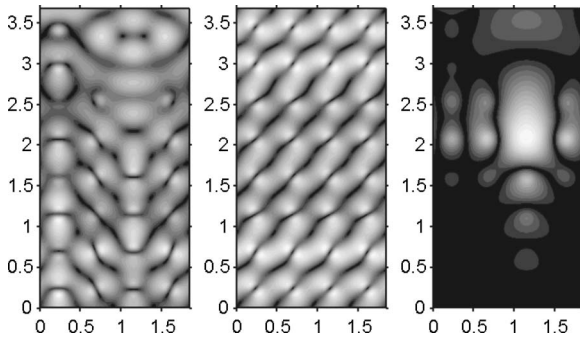


FIG. 10. Electric field within the region $0 \leq x \leq L$, $0 \leq y \leq Na$ at $kL=16.97$ and the same other parameters as in Fig. 8(a) (left) and in Fig. 8(b) except for $\theta=21.7^\circ$ (middle) and at 7.44 and the same other parameters as in Fig. 9 (right). Brighter regions correspond to larger field values, $\max|E|/|E_0^i| \approx 2.9$ (left), 3 (middle), and 14 (right).

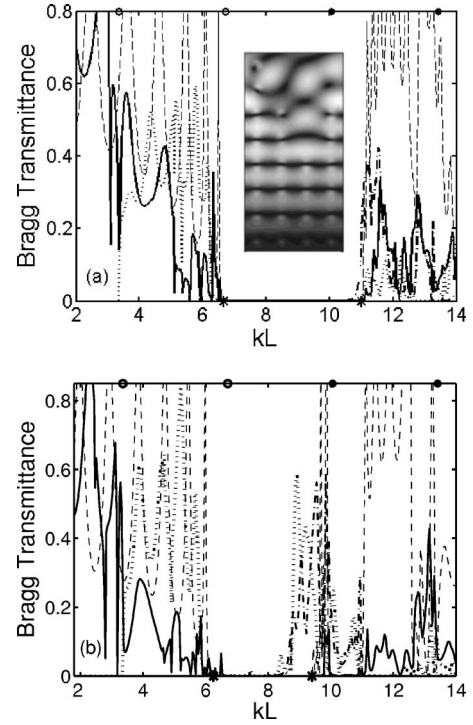


FIG. 11. Transmission with different Bragg beams at $\theta=\pi/3$, $\varepsilon_h=1.0$ (a), $\varepsilon_h=2.1$ (b), and the same other parameters as in Figs. 4(a) and 9, respectively. Thick solid, dotted, and dash-dotted lines show t_0 , t_{-1} , and t_{-2} , respectively. Thin dashed lines show t_0 for the noncorrugated PC. Circles correspond here to $k_c^n(L, \theta)$ at $n=-1, -2, -3$, and -4 ; kL values with $t_0/W=2.5 \times 10^{-3}$ at the edges of the opaque range of T for the noncorrugated PC are shown by asterisks. The inset in case (a) shows the field pattern at $kL=11$; $\max|E|/|E_0^i| \approx 2.2$, $t_{-2} \approx 0.16$.

given rule of the signature of the nonordinary behavior. At the right edge of the ordinary opaque range, the transmitted beams are strongly deflected as compared to the incidence direction. For example, in Fig. 11(a), T_{-2} only contributes to T at

$$\kappa_c^{-2} < k < \hat{\chi}_u^{(nc)}(\pi/3) \approx \kappa_c^{-1} \approx \kappa_c^0, \quad (19)$$

where $\hat{\chi}_u^{(nc)}(\pi/3)$ is the upper boundary of the opaque range of the noncorrugated PC with the same number of layers. ϕ_{-2} varies from 19.3° to 16° while (19) is satisfied. This means that the only transmitted beam has the opposite sign of k_x compared to the incident one. Hence an effect is realized here which is similar to negative-index refraction (NIR). However, in contrast with NIR, we observe our effect not at an interface between two media, but as the common effect of both interfaces of a finite-thickness PC. It can be referred to as *negative deflection*. The inset in Fig. 11(a) shows the field pattern at the right boundary of the range given by (19). In Fig. 11(b), two beams T_{-1} and T_{-2} contribute to T at the right edge of the ordinary opaque range, while T_0 is suppressed. Here $\phi_{-1}=-12^\circ$ and $\phi_{-2}=26.7^\circ$, so that T_{-2} is deflected with changing the sign of k_x , while T_{-1} does so without changing this sign.

An increase of d/a and/or ε_r can result in the appearance of several ordinary opaque ranges within the considered range of kL variation, while the boundaries of the opaque ranges for individual beams can still be different. This situation has been observed, for example, at $\varepsilon_r=14$, $d/a=0.6$, and the same other parameters as in Fig. 4(a). Contrary to Fig. 4(a), the case for

$$\chi_l < k_c^{\pm 1}(L, 0) < \chi_u < \kappa_c^{\pm 1}(0)$$

was realized at these parameters without the appearance of any weak peak of t_{-1} at the left edge. All of the above-discussed features have been observed at $a=L/4$ and $0.95 < L/\lambda < 3$ where λ is the free-space wavelength. Hence the condition $a \ll L \propto \lambda$ used in [29] is not necessary to obtain a periodic structure where some propagative beams T_n would be suppressed. Note that t_n might take larger values at the peaks than those in the figures presented if the step over kL is decreased.

B. Metallic structures

The dispersion and transmission properties of two-dimensional metallic PC's have been studied in many papers—e.g., see [3,43–45]. For example, some peculiar effects like band flattening, band broadening, and the possibility of the appearance of an infinite number of surface plasmon modes have been demonstrated in [45]. Here we study transmission through structures which are similar to those considered in Sec. III A, but differ in that the rods are made of a material whose permittivity is described in the framework of Drude's model. In Figs. 12(a) and 12(b), DE values vs kL are presented for the same geometrical parameters as in Figs. 4(a) and 9, respectively, while ε_r is given by Eq. (14). Examples of the near-field pattern which are typical for the vicinity of the edge of the opaque range are shown in the insets. The mechanism of the appearance of the lowest opaque ranges here differs from that in Sec. III A. It is connected to the range of ω variation where ε_r is negative according to Eq. (14). A plasmonic opaque range occurs in the transmittance of a homogeneous noncorrugated metallic slab. For an array of metallic rods, this effect can be scaled down to smaller ω , so that the opaque range can be bounded by an effective frequency $\omega = \omega_{p,eff} < \omega_p$ [40,46].

At the edge of such an opaque range, some effects appear which are similar to those observed at the edges of the lowest opaque range in the above-considered dielectric PC's. In particular, the actual cutoffs can be shifted towards larger kL . Furthermore, the shifts are different for different diffraction orders, so that *each order or pair of the orders has, in fact, its own opaque range*. Thus one can distinguish between the ordinary ($T=0$) and nonordinary ($t_n \neq 0$ or $t_n=0$ only for one of the n values if $\theta \neq 0$ or for a pair of the values $\pm n$ if $\theta = 0$) plasmonic opaque ranges.

In Fig. 12(a), we observe a situation that only T_0 is actually contributive to \mathcal{T} at those k for which

$$k_c^{\pm 1}(L, 0) < \kappa_c^0(0) < k < \kappa_c^{\pm 1}(0),$$

where $\kappa_c^0(0)=6.8$ and $\kappa_c^{\pm 1}(0)=9.3$. By analogy with the examples presented in Sec. III A, an increase of ε_h results in a

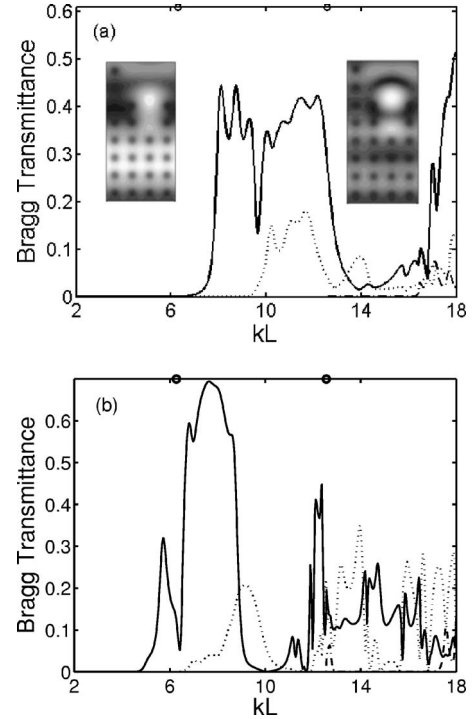


FIG. 12. Transmission with different Bragg beams at $\varepsilon_h=1.0$ (a), $\varepsilon_h=2.1$ (b), $\omega_p L/c=8.5\pi$, $\gamma/\omega_p=0.01$, $d/a=0.4$, $N=8$, $\theta=0$, $L=4a$, $A=0.79$, $B=0.21$, $C=D=0$, and $\varphi_1=-\pi/4$. Solid, dotted, and dash-dotted lines correspond to t_0 , $t_{\pm 1}$, and $t_{\pm 2}$, respectively. Circles show the values of $k_c^n(L, \theta)$ at $n=\pm 1$ and $n=\pm 2$. Left and right insets in case (a) show the near-field pattern at $kL=8$ ($t_0 \approx 0.38$) and 8.7 ($t_0=0.44$), respectively; brighter regions correspond to larger field values, $\max|E|/|E_0| \approx 2.5$ and 3.2 for the left and right insets.

shift of the right edges of the opaque ranges—compare Fig. 12(a) to Fig. 12(b). In case (b), the values of $k_c^n(L, 0)$ at $n = \pm 1$ are just slightly smaller than $\kappa_c^n(0)$, while the value of $\kappa_c^0(0)$ is also shifted towards smaller k . Besides, the extended nonordinary range with suppressed $T_{\pm 2}$ does appear.

An increase of θ leads to the plasmonic cutoffs of lower orders being faster shifted towards larger kL than those of higher orders. As a result, a new type of nonordinary behavior can appear when

$$\kappa_c^n(\theta) \leq \kappa_c^0(\theta), \quad (20)$$

where $n=-p, -p+1, \dots, 0, 1, \dots, s$. Hence the order of the actual cutoffs can be changed as compared to the classical theory of gratings. These results are illustrated by Fig. 13, where T_{-1} dominates at the edge. Varying ε_h and/or corrugation parameters, one can obtain the case that

$$\kappa_c^0(\theta) \approx \kappa_c^{-1}(\theta) \approx \kappa_c^{-2}(\theta), \quad (21)$$

while only the orders T_0 , T_{-1} , and T_{-2} are propagative. Note that in case (a), $\mathcal{T} \approx t_0$ at $kL=13.4$, while the nonordinary range with suppressed T_{-1} and T_{-2} extends from $kL \approx 14$. The rule of signature of the nonordinary behavior, which has been used above for the dielectric PC's, can be used for the metallic PC's, too.

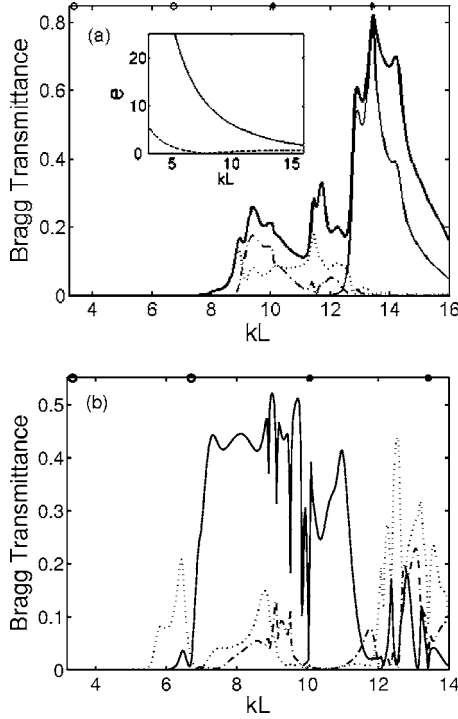


FIG. 13. Same as in Fig. 12 but for $\theta = \pi/3$. Open circles: $\kappa_c^n(L, \theta)$ at $n = -1$ and $n = -2$. Solid circles: $\kappa_c^n(L, \theta)$ at $n = -3$ and $n = -4$. In case (a), the thick solid line shows \mathcal{T} . The inset in case (a) shows $e = |\text{Re } \epsilon_r|$ vs kL at $\omega_p L/c = 8.5\pi$ (solid line) and $\omega_p L/c = 2.5\pi$ (dashed line), $\gamma/\omega_p = 0.01$.

In Fig. 13(a), T_0 is suppressed at the edge of the opaque range of \mathcal{T} . At $\kappa_c^{-1} < k < \kappa_c^{-2}$, ϕ_{-1} varies from -4.6° to -8.3° . At $\kappa_c^{-2}L = 8.7$, $\phi_{-2} = 35.3^\circ$. Hence we again obtain the situation that two contributive beams show an opposite sign of k_x [compare to Fig. 11(b)]. Furthermore, T_{-2} can dominate in \mathcal{T} , as occurs in Fig. 13(a) at $9.03 < kL < 10.1$. In Fig. 13(b), the only contributive beam at the edge is negatively deflected [compare to Fig. 11(a)]. For example, $\phi_{-1} = 16^\circ$ at $kL = 5.5$.

For comparison, Fig. 14 shows t_0 and t_{-1} for the noncorrugated PC with the same parameters as in Figs. 12(a) and 13(a), except for A, B, C , and D . One can see that the second opaque range appears in the vicinity of $kL = 15$ at $\theta = 0$. A

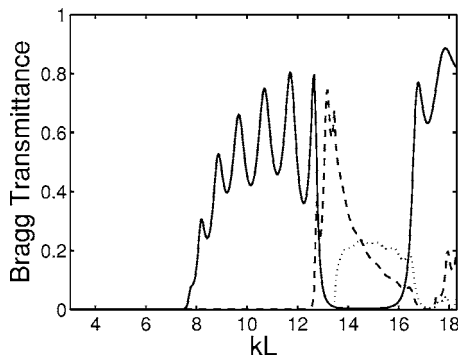


FIG. 14. Bragg transmittance for a metallic PC with linear interfaces at $A=1, B=C=D=0, \epsilon_h=1, \omega_p L/c=8.5\pi, \gamma/\omega_p=0.01$, and $d/a=0.4$. Solid, dashed, and dotted lines correspond to $\mathcal{T}=t_0$ at $\theta=0$ and to t_0 and t_{-1} at $\theta=\pi/3$, respectively.

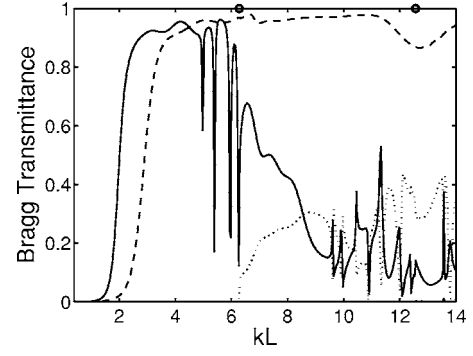


FIG. 15. Transmission with different Bragg beams at $\epsilon_h=2.1, \omega_p L/c=2.5\pi, \gamma/\omega_p=0.01, d/a=0.4, N=8, \theta=0, L=4a, A=0.79, B=0.21, C=D=0$, and $\varphi_1 = -\pi/4$. Solid, dotted, and dash-dotted lines correspond to $t_0, t_{\pm 1}$, and $t_{\pm 2}$, respectively. For the dash-dotted line, $t_{\pm 2} \approx 0$. Dashed line: $t_0 \approx \mathcal{T}$ in case with the same parameters except for $\epsilon_h=1.0$. Circles: $\kappa_c^n(L, 0)$ at $n \pm 1$ and $n \pm 2$.

similar range occurs at $kL=21$ for $\theta=\pi/3$. These ranges disappear as soon as a rather large part of the rods is removed from the upper interface. It is interesting to compare the values of $\kappa_c^0(\theta)$ in Figs. 12(a), 13(a), and 14. In the case of $\theta=0$, they differ rather slightly for the corrugated and noncorrugated PC's. On the other hand, a substantial shift of the cutoff of \mathcal{T} towards smaller values takes place due to the corrugation at $\theta=\pi/3$, which is in agreement with the above-mentioned rule. It is worth noting that the nonordinary range in Fig. 13(a) at $kL > 14$ partially coincides with the range in the vicinity of $kL=15$ in Fig. 14, where $\mathcal{T} \approx 0$ at $\theta=0$, but $\mathcal{T} > 0.2$ at $\theta=\pi/3$. The same holds true concerning the range with dominating T_0 in the vicinity of $kL=10.5$ in Fig. 13(b) and the θ -dependent opaque range for the corresponding noncorrugated PC.

The effect of decreasing ω_p is illustrated in Fig. 15. The main features which distinguish this case from the previous ones are the weakening contribution of higher orders, which occurs at least at $\epsilon_h=1.0$, and increasing \mathcal{T} due to decreasing losses. In the case of $\epsilon_h=1.0$ in Fig. 15, the transmission $\mathcal{T} \approx t_0$ can approximately be characterized in terms of $n_{\text{eff}}(k)$, even at $k > \kappa_c^{-1}(0)$. One can see that the presence of a nonair host medium is necessary to let higher orders be actually contributive. Note that at $\epsilon_h=2.1$ and $kL \approx 11.25$, $\mathcal{T} \approx 0.96$, $t_0 = t_{\pm 1} = 0.32$, so that an appropriate splitting regime can be realized. At $\theta \neq 0, \epsilon_h=1.0$, and the same other parameters as in Fig. 15, the situation still occurs when $\kappa_c^n(\theta)$ values are shifted in the vicinity of the edge of the plasmonic opaque range in such a manner that

$$\kappa_c^{-1}(\theta) \leq \kappa_c^0(\theta).$$

As follows from the comparison of the results presented in Fig. 15 with those obtained for a solid grating at $\epsilon_r = \epsilon_h = 2.1$, scattering either by the rods or by the dielectric grating dominates in the total scattering within different ranges of kL variation. Hence the similarity can be seen between this case and that observed in Fig. 2(a) of [47], where either the effect of effective surface or the effect of particles under a flat

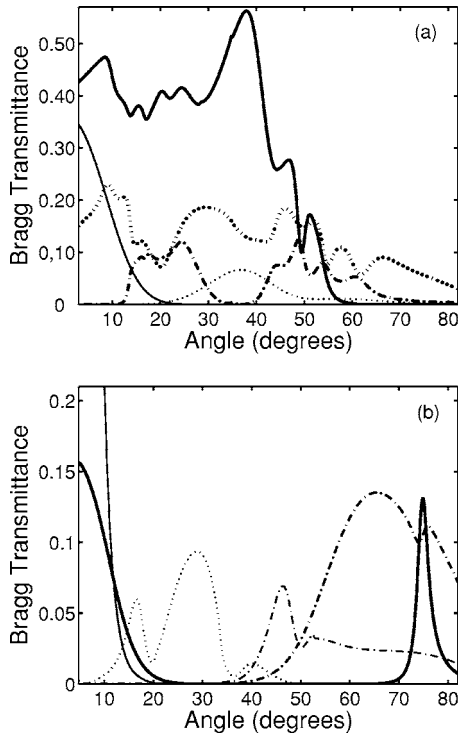


FIG. 16. Transmission with different Bragg beams vs θ . Solid, dotted, and dash-dotted lines show t_0 , t_{-1} , and t_{-2} , respectively. In case (a), thick and thin lines correspond to $kL=12$ and 8, respectively; ϵ_r is given by Eq. (14) where $\omega_p L/c=8.5\pi$ and $\gamma/\omega_p=0.01$. In case (b), thick lines correspond to $\epsilon_r=5.8$ and $kL=12$ (here t_{-1} is not shown, $t_{-1}<0.013$); thin lines correspond to $\epsilon_r=14$ and $kL=14$. In all cases, ϵ_h , d/a , N , m , A , B , C , D , and φ_1 are the same as in Figs. 4(a) and 12(a).

surface was dominating in the whole reflected intensity within different ranges of θ variation.

Since a lossless plasmonic material cannot be realized ($\gamma>0$), any metallic PC should be carefully designed. In various kL ranges, taking a value of $\epsilon_h>1$ instead of $\epsilon_h=1$ can lead to either an increase or a decrease of the losses. Note that the effects related to higher opaque ranges are expected to be more strongly pronounced for another N , f_0 , f_1 , and $\omega_p L/c$ than in Figs. 12, 13, and 15. To let the demonstrated nonordinary effects be pronounced, the same condition is necessary as in the dielectric case: The upper interface has to be corrugated.

C. Angular dependence

Finally, we consider briefly typical features of the θ dependence of DE's. Figure 16 demonstrates some of them for the same material and/or geometrical parameters as those used above. In particular, low-pass and band-stop kinds of behavior of t_n vs θ are typical [e.g., see thin solid line in case (a) and thick solid line in case (b)]. In the case shown in Fig. 16(a) by thick lines, T_0 is allowed to propagate but is suppressed at $\theta>60^\circ$ and T_{-2} does so at $2.7^\circ<\theta<11.8^\circ$ and at $35.1^\circ<\theta<38.7^\circ$. The propagative orders T_1 and T_{-3} (not shown) also contribute to \mathcal{T} at $\theta<20^\circ$ and in the vicinity of

$\theta=34.8^\circ$, respectively. In the former case, $\max t_1\approx 0.12$ at $\theta=0$.

In the case shown in Fig. 16(a) by thin lines, the opaque ranges are observed for the propagative orders T_0 and T_{-1} at $\theta>19.5^\circ$ and $\theta<22.1^\circ$, respectively. T_{-2} and T_1 may propagate at $\theta>34.8^\circ$ and at $\theta<12.4^\circ$, respectively, but are suppressed for all θ . One can consider the ranges with suppressed propagative orders as the θ -domain analogs of the nonordinary opaque ranges, which have been observed in the kL dependence of t_n . In some cases, such ranges represent an extension of a narrower range, within which the propagation is forbidden because (4) is not satisfied. Note that the opaque ranges can appear in the θ domain in both cases of dielectric and metallic rods.

In the case shown in Fig. 16(b) by thick lines, propagative orders T_0 and T_{-2} are suppressed at $22.1^\circ<\theta<69.3^\circ$ and $2.7^\circ<\theta<40.4^\circ$, respectively. The orders T_1 , T_2 , T_{-3} , and T_{-4} , which are allowed to propagate within a certain θ range, are nevertheless suppressed. In the case of thin lines, the opaque ranges occur at $\theta>46.5^\circ$ (T_{-1}), $\theta<36.4^\circ$ (T_{-2}), and $\theta>18.4^\circ$ (T_0). The narrow peak of $t_1\approx 0.04$ at $\theta\approx 26^\circ$ and that of $t_{-3}\approx 0.045$ at $\theta\approx 37^\circ$ are not shown, since the effect of these DE's on \mathcal{T} is restricted to a very narrow range.

Note that the low-pass behavior of t_0 vs θ (thin solid lines) is similar to that observed in the periodic structures with metallic rods and linear interfaces, which behave like an ultralow-permittivity slab, $\epsilon_{eff}<1$ [48]. However, we also observe contributive higher orders, while the effect of T_0 either weakens or can be neglected at all. Hence, this behavior is even more similar to that which has been observed by the authors for the finite-thickness periodic structures made of a homogeneous ultralow-permittivity material [29]. Dependences shown in Fig. 16(b) by thin lines are rather close to those obtained at $kL=2\pi$ and the same other parameters as in Fig. 2 of [29] (these curves have not been shown in [29]). One can expect that a special type of effective behavior might appear in the considered PC, which is related to the multibeam regime.

IV. CONCLUSIONS

In this paper, we have studied the transmission of *s*-polarized plane waves through rather thin PC's with a curvilinear, periodically corrugated interface. As follows from the obtained results, purely dielectric corrugated PC's borrow the features of transmission characteristics from both conventional dielectric PC's and gratings, at those parameters at which a multibeam regime may exist. Several interesting effects can be realized due to the interface modulation. In parallel with ordinary opaque ranges for which transmission is vanishing for any Bragg beam, nonordinary opaque ranges can appear for certain performances, where only one or a pair of formally propagative orders remains contributive while others are suppressed. In some cases, nonordinary behavior has been observed at the edges of an ordinary opaque range, leading to an extension of the opaque ranges for one or several orders. We have demonstrated that the numbers of beams in the half-spaces above and below the PC can be different owing to both nonordinary effects.

The presence of corrugation at the upper interface is the necessary condition for the appearance of these effects. Any nonordinary behavior has not been observed for noncorrugated PC's. Both these statements remain true at least within the considered range of parameter variation. A shift of the actual cutoffs towards larger frequencies in comparison with the Rayleigh cutoffs is realized due to the ordinary opaque ranges, but it can be further increased due to the nonordinary effects if the upper interface is corrugated. The detected features of transmission are beyond the classical theory of optical gratings. On the other hand, they are not typical for the conventional finite-thickness PC's.

It follows from the obtained results that at least four mechanisms of establishing these nonordinary effects can be distinguished, depending on the role played by the corrugation in the formation of the near-field pattern. This role can be the following: (i) perturbation of the field of the noncorrugated PC within a pass band at a given θ ; (ii) variation of the field structure, at least for most part of the corrugated PC, in order to imitate the incidence at a certain equivalent angle(s) θ_e , at which transmission through the noncorrugated PC is possible, in contrast with the actual θ ; (iii) local enhancement of the field at the corrugation grooves (defect mode of a special type) and further tunneling through the PC. Understanding the transmission mechanism in the fourth case, which is realized at the left edge of the ordinary opaque range, requires performing an additional study for thin noncorrugated PC's.

Varying the corrugation parameters and the permittivity of the rods and host medium, one can control the DE values of the propagative diffraction orders, the boundaries of the opaque ranges, and the number of actually contributive orders. In this context, it is worth mentioning the cases when all transmitted beams are deflected, as well as a purely negative deflection.

Most of these effects have also been observed in the structures with metallic rods, whose permittivity is described in the framework of Drude's model. In this case, the lowest opaque range appears at $\omega < \omega_{p,eff}$ due to a ϵ_r -negative behavior, irrespective of the number of formally propagative orders. As in the dielectric case, nonordinary behavior at the edge is possible, so that the cutoffs of individual beams can be shifted towards higher frequencies as compared to $\omega_{p,eff}$. Furthermore, the sequence of actual cutoffs of the individual diffraction orders can differ from the conventional sequence of the Rayleigh cutoffs. In particular, a higher order can be contributive, while a lower order does not yet.

In the angular dependence of DE values, analogs of the nonordinary effects observed in the frequency dependence have also been detected. Among various cutoff-type dependences, one should mention that one which is similar to the behavior observed recently in the scattering by a homogeneous ultralow-permittivity slab with a corrugated interface. This similarity looks promising for realization of an effective behavior of the corrugated PC's, while more than one diffraction order contributes to the transmission.

-
- [1] K. Sakoda, *Optical Properties of Photonic Crystals* (Springer, Berlin, 2001).
- [2] *Photonic Crystals: Physics, Fabrication and Applications*, edited by K. Inoue and K. Othaka (Springer, Berlin, 2004).
- [3] M. M. Sigalas, C. T. Chan, K. M. Ho, and C. M. Soukoulis, *Phys. Rev. B* **52**, 11744 (1995).
- [4] O. Toader and S. John, *Phys. Rev. E* **70**, 046605 (2004).
- [5] C. Luo, S. G. Johnson, J. D. Joannopoulos, and J. B. Pendry, *Phys. Rev. B* **65**, 201104(R) (2002).
- [6] S. Enoch, G. Tayeb, and D. Maystre, in *Progress in Electromagnetics Research*, edited by J. A. Kong (EMW, Cambridge, MA, 2003), Vol. 41, pp. 61–81.
- [7] I. Alvarado-Rodriguez, P. Halevi, and A. S. Sanchez, *Phys. Rev. E* **63**, 056613 (2001).
- [8] H. Benisty *et al.*, *J. Lightwave Technol.* **17**, 2063 (1999).
- [9] M. Yan, P. Shum, and J. Hu, *Opt. Lett.* **30**, 465 (2005).
- [10] Z.-Y. Li and K. M. Ho, *Phys. Rev. Lett.* **92**, 063904 (2004).
- [11] S. Kim, I. Park, and H. Lim, *Opt. Lett.* **30**, 257 (2005).
- [12] J. R. Sirigiri, K. E. Kreischer, J. Machuzak, I. Mastovsky, M. A. Shapiro, and R. J. Temkin, *Phys. Rev. Lett.* **86**, 5628 (2001).
- [13] N. Garcia, E. V. Ponizovskaya, and J. Q. Xiao, *Appl. Phys. Lett.* **80**, 1120 (2002).
- [14] B. Gralak, S. Enoch, and G. Tayeb, *J. Opt. Soc. Am. A* **17**, 1012 (2000).
- [15] R. W. Ziolkowski, *Phys. Rev. E* **70**, 046608 (2004).
- [16] P. V. Parimi, W. T. Lu, P. Vodo, J. B. Sokoloff, J. S. Derov, and S. Sridhar, *Phys. Rev. Lett.* **92**, 127401 (2004).
- [17] S. Foteinopoulou, E. N. Economou, and C. M. Soukoulis, *Phys. Rev. Lett.* **90**, 107402 (2003).
- [18] C. H. Kuo and Z. Ye, *Phys. Rev. E* **70**, 056608 (2004).
- [19] X. Wang, Z. F. Ren, and K. Kampa, *Appl. Phys. Lett.* **86**, 061105 (2005).
- [20] Z.-Y. Li and L.-L. Lin, *Phys. Rev. B* **68**, 245110 (2003).
- [21] P. Vodo, P. V. Parimi, W. T. Lu, and S. Sridhar, *Appl. Phys. Lett.* **86**, 201108 (2005).
- [22] S. K. Morrison and Y. S. Kivshar, *Appl. Phys. Lett.* **86**, 081110 (2005).
- [23] L. Wu, *Appl. Phys. Lett.* **86**, 211106 (2005).
- [24] N. Horiuchi, Y. Segawa, T. Nozokido, K. Mizuno, and H. Miyazaki, *Opt. Lett.* **30**, 973 (2005).
- [25] T. D. Happ, M. Kamp, and A. Forchel, *Opt. Lett.* **26**, 1102 (2001).
- [26] C. Li and Z. Chen, in *Progress in Electromagnetics Research*, edited by J. A. Kong (EMW, Cambridge, MA, 2003), Vol. 42, pp. 91–105.
- [27] R. W. Ziolkowski and A. D. Kipple, *IEEE Trans. Antennas Propag.* **51**, 2626 (2003).
- [28] R. A. Depine and A. Lakhtakia, *Phys. Rev. E* **69**, 057602 (2004).
- [29] A. E. Serebryannikov, T. Magath, K. Schuenemann, and O. Y. Vasylichenko, *Phys. Rev. B* **73**, 115111 (2006).
- [30] R. A. Depine, A. Lakhtakia, and D. R. Smith, *Phys. Lett. A* **337**, 155 (2005).

- [31] S. Foteinopoulou and C. M. Soukoulis, Phys. Rev. B **67**, 235107 (2003).
- [32] K. Sakoda, Phys. Rev. B **52**, 8992 (1995).
- [33] S. Foteinopoulou and C. M. Soukoulis, Phys. Rev. B **72**, 165112 (2005).
- [34] X. Yu and S. Fan, Phys. Rev. E **70**, 055601(R) (2004).
- [35] *Electromagnetic Theory of Gratings*, edited by R. Petit (Springer, Berlin, 1980).
- [36] T. Magath and A. E. Serebryannikov, J. Opt. Soc. Am. A **22**, 2405 (2005).
- [37] K. Sakoda and H. Shiroma, Phys. Rev. B **56**, 4830 (1997).
- [38] D.-Y. Jeong, Y. H. Ye, and Q. M. Zhang, J. Appl. Phys. **92**, 4194 (2002).
- [39] T. Ueda, K. Othaka, N. Kawai, and K. Sakoda, J. Appl. Phys. **84**, 6299 (1998).
- [40] J. B. Pendry, A. J. Holden, W. J. Stewart, and I. Youngs, Phys. Rev. Lett. **76**, 4773 (1996).
- [41] The number of propagative orders above the relief grating can be smaller (larger) than below it if the grating material is optically more (less) dense than air. For example, see Chap. 1.3 in [35].
- [42] W.-C. Tan, T. W. Preist, and R. J. Sambles, Phys. Rev. B **62**, 11134 (2000).
- [43] G. Guida, D. Maystre, G. Tayeb, and P. Vincent, J. Opt. Soc. Am. B **15**, 2308 (1998).
- [44] E. Moreno, D. Erni, and C. Hafner, Phys. Rev. B **65**, 155120 (2002).
- [45] R.-L. Chern, Chien C. Chang, and C. Chung Chang, Phys. Rev. E **73**, 036605 (2006).
- [46] We assume that the effective frequency can be introduced as $\omega_{p,eff} = c \min \kappa_c^n(0)$ whatever the number of formally propagative orders.
- [47] A. Sentenac, H. Giovannini, and M. Sailard, J. Opt. Soc. Am. A **19**, 727 (2002).
- [48] B. T. Schwartz and R. Piestun, J. Opt. Soc. Am. B **20**, 2448 (2003).